where *u* is the average velocity, *g* is gravitational acceleration and *h* is flow depth). Grant (1997) provided the first assessment of such an interaction on high-gradient alluvial channels. He showed that *Fr* could not be higher than unity over long distances or long periods of time. The same interaction was demonstrated by Gimenez and Govers (2001) on eroding rills. Finally, Gimenez *et al.* (2004) hypothesized that critical flow was a necessary condition for rill initiation. Interaction with *Fr* lies on the development of small hydraulic jumps along the rill when the flow velocity is critical. At the jump location, localized erosion occurs due to turbulence in the jump, with the result of eroding the channel, enlarging it and finally lowering the average velocity above the critical speed.

This knowledge of rill initiation and development is however underexploited in most erosion models. Rill density is either predefined (one rill per metre for WEPP: Gilley *et al.* 1988) or as an input parameter (Siepel *et al.*, 2002). A few models are aimed at dynamically developing a rill network (RillGrow model, Favis-Mortlock *et al.*, 2000; PSEM_2D model, Nord and Esteves, in press) However, these models use uniform friction factors. Finally little attention had been paid to the reliability of *Re* and *Fr* values simulated by erosion models.

This study presents a rainfall-simulation experiment carried out at Thies, Senegal (14º45′43″N, 16º53′16″W), on a 40-m^2 plot with sandy soil and low slope (1%). Flow velocity was measured at 58 individual points on the plot with a miniaturized version of the salt velocity gauge (SVG) technology (Planchon *et al.* 2005). SVG is an automated salt-tracing technique which provides reliable point velocity data over a wide range of flow speeds and with no lower limit on flow depth. Measured velocities have been compared with simulated data from three models and the consequences on the simulation of *Re* and *Fr* are assessed and discussed. The results allow us to draw some research perspectives for the modelling of rill initiation.

Material and methods

The new generation of SVG

The SVG technology has been presented in Planchon *et al.* (2005). It consists of injecting salty brine into the flow and recording the conductivity peak simultaneously at two locations downstream. A new generation of SVG has been developed for this experiment. Each conductivity sensor consisted of two aluminium pins spaced 1-cm apart, which allowed for measuring the velocity of a narrow flow path. The inter-probe distance was 10cm. The flow velocity was calculated by fitting a 1D convection-dispersion model for velocity and dispersion coefficients (Eq. 1). Hayami (1951), reported by Henderson (1966), gave Eq. 2 as the solution of Eq. 1 when C(0,t) is the Dirac function, *i.e.* injection is instantaneous. Eq. 3 describes the least-squares sum that is minimized in the model used by the SVG.

$$\frac{\partial}{\partial} = \frac{\partial}{\partial} \quad \frac{\partial^2}{\partial^2} \tag{1}$$

(2)

(3)

where C is salt concentration (g· l^{-1}); C_1 is measured at the upper probe; C_2 is measured at the down probe; t is time (s); x is length (m); V is flow velocity (m·s^{-1}); $\underline{D}$ is dispersion (m^2·s^{-1}); ⊗ is the convolution product; $\overline{C}$ is Hayami's solution from Eq. 2 with x being the inter-probe distance, i.e. 0·1m; a and b are coefficients that account for salt losses between the two probes (due to infiltration or other cause); *ssq* is the quadratic sum that is minimized by fitting V, D, a and b for each pair of peaks.

The new generation of SVG requires two operators. The first is located on the plot to place the probes in the measuring locations and to do the injections manually. The brine was coloured with potassium permanganate to allow for visual control of the tracing process. Four probes were multiplexed to the datalogger, allowing four locations to be measured simultaneously. The second operator was at the computer. At a given signal, the data acquisition was triggered when the first operator injected the brine a few centimetres upstream of the probes. Conductivity was measured at 200 Hz during 2·5s and the model was then automatically fitted to the data. The measurement was replicated until clear peaks were seen on the software graphical interface and the model gave satisfactory results.

Rainfall-simulation experiment

The rainfall-simulation site was located at Thies, Senegal. The plot was 10m long by 4m wide, with a 1% slope, and sandy soil (1% clay, 7% silt, 43% fine sand, 49% coarse sand). The rainfall simulator was as described by Esteves *et al.* (2000a). It allowed for

rainfall at constant intensity of 70mm $\cdot hr^{-1}$ in average. In order to limit wind effects, which may cause noticeable variations of rainfall intensity, simulations were carried out at a maximum wind speed of 1 $m \cdot s^{-1}$. Six tipping-bucket rain gauges with electronic recording were placed along the plot borders for monitoring the actual rainfall intensity. The flow discharge was collected in a trough and alternately directed, via a 4-inch flexible hose, into two 150-litre cylindrical buckets, one being filled while the other was drained. The volume in the filling bucket was monitored by recording the rise of a float. The resolution of this apparatus was 2·5litres. The typical flow discharge at steady state was 0·5l $\cdot s^{-1}$.

On day 1 of the experiment, a wetting rainfall of 20mm was applied and the plot was manually ploughed to a depth of 50cm. The surface was then raked in order to form a slight V shape, with 1% slope longitudinally and 1% slope towards the median axis of the plot. The purpose of the V shape was to prevent a rill from forming by the edge of the plot.

The experiment detailed in this article was held on day 7. The days before, a total of six hours of rainfall had already been applied on the plot for others experiments that are not reported in this article. The consequence of these successive experiments was an already 'old' surface with a well organized flow pattern. The longitudinal slope had evolved from straight to slightly concave (Figure1) with thick sand deposits in the concave downstream part.

Days 6 and 8 (*i.e.* the day before the experiment, and the day after) were used to carry out microrelief measurements. The relief-meter was the same as described by Planchon *et al.* (2001). It consists of a vertical rod with a sensor at the end that detects the soil surface. Stepper motors allow the apparatus to move in small increments in all directions. The horizontal resolution is 2·5cm transversally to the plot and 5cm longitudinally . The vertical precision is 0·5mm. With a maximum acquisition rate of 1·6 point· s^{-1}, the 16,000 measured points of the entire plot required a full day.

The experiment on day 7 consisted of a 2h15'-long continuous rainfall at constant rainfall intensity (69 $mm \cdot h^{-1}$ on average). After the discharge had stabilized, flow velocity was measured at 72 locations with three to six replications, which led to a total of 348 individual velocity measurements. Among this set, 122 individual measurements, covering 68 locations, have been selected for further analysis. The other data were discarded for various reasons: in particular because of the poor quality of either one of the two conductivity peaks or poor quality of the modelled peaks.

At the end of the experiment, a series of digital pictures of the plot were taken from a height of 6 metres above the plot. The pictures have been mounted in a single file and geometrically corrected so that each pixel corresponds to one square millimetre in the field. The resulting image can be combined with a DEM to calculate virtual pictures. Figure1 shows one of these views with the relief magnified ten times and the colour contrast enhanced. The native soil appears in black (its natural colour is a yellowish light brown). White and reddish colours correspond to various types of sand deposits.

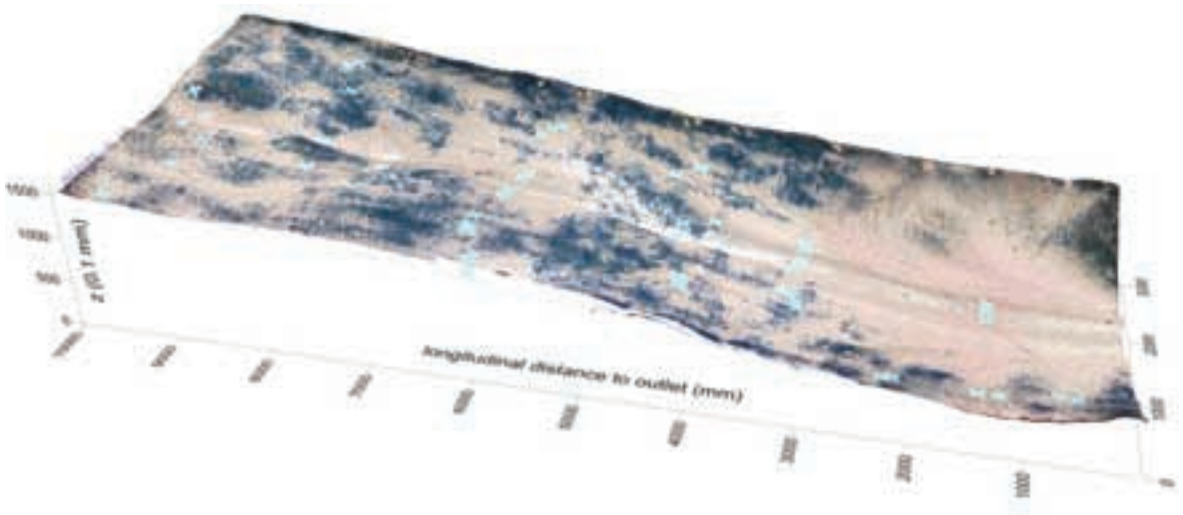

Figure. 1. Location of the velocity measurements showed on a virtual picture of the plot. Vertical axis has been magnified ten times. Colour contrast has been enhanced. The native soil appears in black. White and reddish colours correspond to various types of sand deposits

The models

PSEM 2D (Plot Soil-Erosion Model 2D; Nord and Esteves, in press; Esteves *et al.*, 2000b) is a soil erosion model dedicated to small experimental plots, typically of less than 100m ^{2}.

Overland flow is described by the depth-averaged two-dimensional unsteady flow equations commonly referred to as the Saint-Venant equations (Zhang and Cundy, 1989). The friction slopes are approximated using the Darcy-Weisbach equation (Eq. 4.) derived for uniform steady flow. The second-order explicit scheme of MacCormack (1969) is used for solving the overland flow equations. Infiltration is computed at each node using a Green-Ampt model (Green and Ampt, 1911).

$$S_{fx} = ff\frac{u_x^2}{8gh}, S_{fy} = ff\frac{u_y^2}{8gh} \quad (4)$$

where *ff* is the calibrated Darcy-Weisbach friction factor. A constant value is assuming during the simulation.

NCF (New Conceptual Framework; Parsons *et al.*, 1997, Wainwright *et al.*, 1999) is a flexible model that can be used for experimental plots as well as small watersheds. The hydraulics consists of solving the kinematic wave equation in 1D along the flow direction derived from a DEM which depressions have been previously filled (using the algorithm from Planchon and Darboux, 2001). The kinematic wave simplification uses the continuity equation from Eq. 5, together with the Darcy-Weisbach equation in one dimension (Eq. 6). The numerical scheme used with this model is the Euler simple backward difference (Scoging, 1992).

$$\frac{\partial q}{\partial x} + \frac{\partial d}{\partial t} = e_x \quad (5)$$

$$v = \sqrt{\frac{8gds}{ff}} \quad (6)$$

where g is gravitational acceleration (m·s^{-2}), d is flow depth (m), q is unit discharge (m^{2}s $^{-1}$) and s is the slope (m·m^{-1}).

The flow is routed from each cell to one of its four adjacent cells in a finite difference grid using a topographically based algorithm based on the greatest difference in altitude of the cells. Overland flow is generated as Hortonian (infiltration excess) runoff by determining the difference between the rainfall and infiltration rate. The latter is predicted using the Smith-Parlange model with modifications to allow runon infiltration and temporally variable rainfall.

RillGrow2 (Favis-Mortlock, 1998; Favis-Mortlock and Boardman, 2000) is a model dedicated to the numerical simulation of emerging rill patterns. Space is discreticized at very small scale so that any cell is supposed to be entirely inside, or entirely outside a rill. Each cell is eroding independently to each other. Cells lower while eroding. Eroding cells thus attract more water flow, subsequently increasing the erosive power of the rill. Because of its high computational needs, applications of RillGrow2 are limited to experimental plots of a few tens of square metres.

RillGrow2 hydraulics consists of calculating a 'potential flow velocity' with a Manning-type equation, based on the water depth: $u = w \cdot d \cdot R^n$, where u is 'potential flow velocity', w is an empirical roughness coefficient, d is water depth, R is the hydraulic gradient and $n = 0{\cdot}5$. The RillGrow2 numerical scheme is unique in soil-erosion modelling: at each time step, the model checks a single cell, chosen at random, and processes it. The check consists of calculating u and determining if outflow is possible from this cell. If the answer is yes, an outlet cell is chosen among eight neighbours according to the steepest descent of the free surface. The required amount of water is then passed from the source cell to the destination cell in order to level the free surface between the two cells. This procedure is then repeated until all cells have been chosen at the particular time step.

Results

Surface-feature patterns

Figure2 shows the left bank of the rill viewed from downstream. The coloured arrows represent the flow velocities as computed by the best model result (to be detailed below). At this point of the result presentation, the model results are used as a convenient illustration of the various flow conditions on the plot and their relation to surface features.

Table 1 summarizes the qualitative information detailed in this section.

Location A represents a high point with a convex soil surface. No visible flow could be seen and the model actually predicts a flow velocity lower than 0·02 m·s^{-1}. Because of their higher position, these locations were sediment sources with regards to splash erosion: sediments occasionally splashed onto these

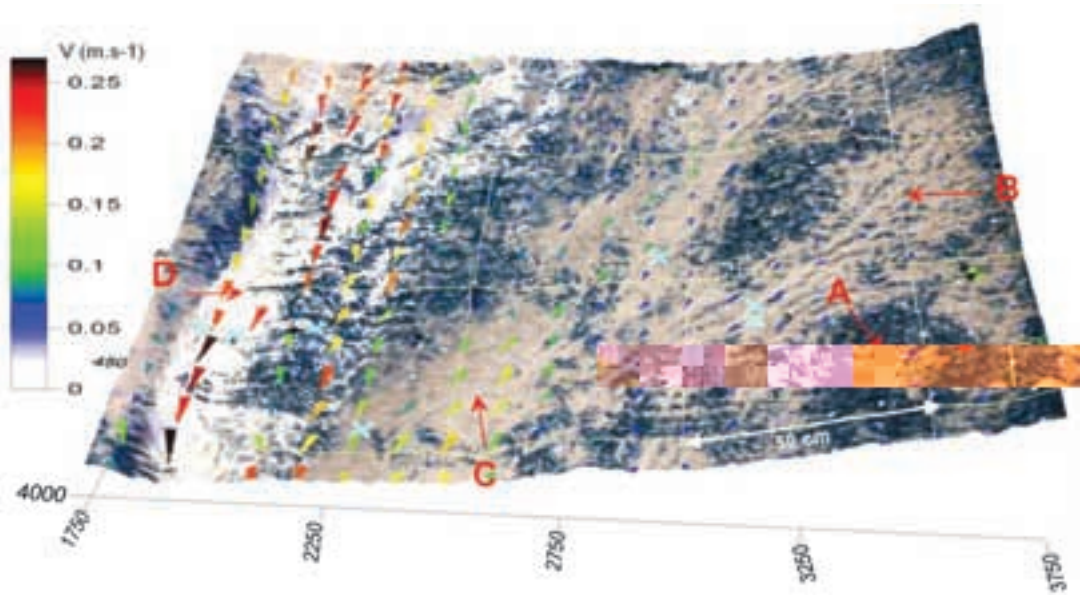

Figure 2. Detail of the left bank of the rill viewed from downstream. Light blue crosses show velocity measurement locations. Coloured arrows are modelled flow velocity. Capital letters show the four surface features that develop on the plot (comments in text). Axis labels are in mm

Table 1. Qualitative information on flow condition deduced from field observation during rainfall and from surface feature description after the experiment

Location	Surface feature	Velocity ($m.s^{-1}$)	Turbulence	Flow regime
A	Native soil, light brown	<0·02	Laminar	Sub-critical
B	Discontinuous sand deposit	0·02 <0·05		
C	Continuous reddish sand deposit	0·1 <0·2	Turbulent	
D	Continuous white sand deposit with crossed wavy features	>0·2		Super-critical

areas were sooner or later splashed back to the lower areas. The soil surface at A had therefore the colour of the native soil, which is a yellowish light brown.

Location B represents the first visible flow. It is characterized by small undulating furrows, ~10 mm wide and 2mm deep. Flow velocity was still slow (~0·05 $m \cdot s^{-1}$ according to the model). The transport capacity was subsequently negligible. However, uneven sand grains could be observed in these tiny channels, slowly creeping downstream until a raindrop hit them and splashed them away. The only turbulence in the flow was caused by raindrop impacts.

At location C, a well established stream was flowing at 0·1 to 0·15 $m \cdot s^{-1}$. The soil surface was covered by a continuous layer of reddish sand that was slowly creeping downstream. Flow was turbulent, but still subcritical. Turbulent flow could easily be determined from the observation of the fate of the coloured brine. In laminar flow, the brine left the injection point very gradually, thus forming a long colourer tail. This fate indicates a vanishing flow velocity at the bottom of the flow, which is typical to laminar flows. In turbulent flows, the tracer left the injection point in a fraction of seconds, indicating a very sharp vertical velocity profile that did not allow the tracer to 'stick' to the soil surface, as it did in laminar conditions.

Location D is characterized by white sand deposits with crossed wavy features typical to supercritical flow. The white colour of the sand indicates that the sand grains were washed up by turbulence until all clay and organic particles had detached. These field observations indicate that the flow was certainly turbulent and supercritical. Modelled as well as measured velocities were all above 0·2m $\cdot s^{-1}$.

Qualitative results

RillGrow2 used 5-cm cells in order to follow its requirement that a given cell should be entirely inside or entirely outside a flow path. NCF used 50-cm cells for the opposite reason: because the 1-D hydraulics does not allow for lateral flow movement, NCF

requires that the same flow path will not be divided into multiple cells, otherwise the modelled free surface may be unrealistic, which leads in practice to numerical instabilities. PSEM_2D used 10-cm cells, which was the smallest cell size the model could simulate without numerical oscillations. Only RillGrow2 was able to run the raw DEM. Both PSEM_2D and NCF needed a smoothed and depression-free DEM.

Each model was calibrated from the hydrograph. The infiltration parameters were calibrated from the total runoff and the steady infiltration rate. The friction factor was calibrated from the hydrograph rise (Figure3).

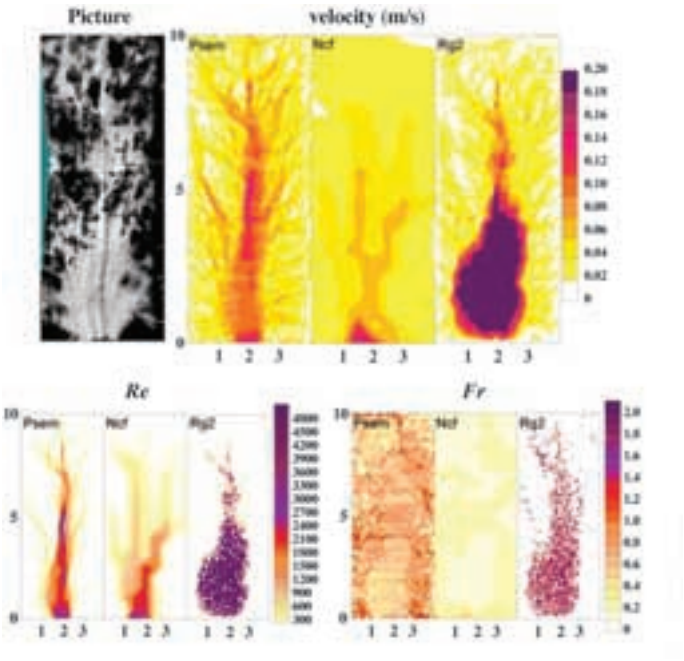

Figure 3. Picture of the plot (with contrast magnified) compared to the velocity, Re and Fr maps predicted by the models. Calibrations were done from the hydrograph

The velocity field from PSEM_2D is very similar to what can be estimated from the picture at the left of the figure. One can notice for example the location of the predicted maximum velocity. It corresponds to the white sands at the centre of the plot, which we interpreted as a mark of supercritical flow. The pattern from NCF is similar to PSEM, with a noticeable loss of precision due to the coarser grid. RillGrow2 predicts a wide area of high velocity in the bottom part of the plot which corresponds fairly well to the concave area of reddish sands deposits that can be seen either on Figures 3 and 1.

The *Re* predictions follow approximately the same pattern as the flow velocity. However, according to the threshold of 2000 commonly used for the transition between laminar and turbulent flows, the spatial extension of turbulent flow is underestimated with regard to observations made by eye during the velocity measurement (as explained in the previous section). *Fr* is even more problematic since no pattern at all is predicted by PSEM_2D or NCF while the pattern predicted by RillGrow2 does not fit to the field observations reported in Table 1.

Models results: Comparison with measured velocity

Figure 4 shows the modelled velocity *vs* the observed ones. All models have a better fit at low velocities than at higher ones. PSEM_2D and NCF slightly overestimate the low velocity and strongly underestimate the high ones. RillGrow2 simulates very well the slowest flows (*i.e.* $v<0 \cdot 05 m \cdot s^{-1}$) and underestimates the other cases. Results from NCF are not exactly comparable to measured data because while measured velocities are point data, the model results represent a $0 \cdot 25\ m^2$ cell. Localized maxima or minima cannot be expected to figure in NCF results.

Modelling the interaction between friction factor and flow conditions

The velocity modelled by PSEM_2D (Figure 4) fits Eq. 8, which can be used to estimate ff_1, the true value of *ff* at each cell. This is done by solving, at each cell, the set of equations 8 to 11 for ff_1, which Eq. 12 gives the solution. Eq. 9 states the unit discharge at the cell location will not change after *ff* is corrected from ff_0 to ff_1. Eq.10 and 1 1 are the Darcy-Weisbach equation before and after correction, respectively.

$$v_0 = b \cdot v_1^{\,a} \tag{8}$$

$$v_0 \cdot h_0 = v_1 \cdot h_1 \tag{9}$$

$$v_0 = \sqrt{\frac{8 g h_0 s}{ff_0}} \tag{10}$$

$$v_1 = \sqrt{\frac{8 g h_1 s}{ff_1}} \tag{11}$$

$$ff_1 = ff_0 \cdot v_0^{\left(3-\frac{3}{a}\right)} \cdot b^{\left(\frac{3}{a}\right)} \tag{12}$$

where $a = 0 \cdot 5$; $b = 0 \cdot 28$; $ff_0 = 0 \cdot 26$; (*h0, v0*) are flow depth and flow velocity read at a given cell in the PSEM_2D results shown in Figures3 and 4; *v1* is the observed velocity; *h1* is the corresponding flow depth according to the modelled unit discharge.

ff_1 was calculated from Eq. 12 at each cell. The resulting map was then smoothed to prevent the model

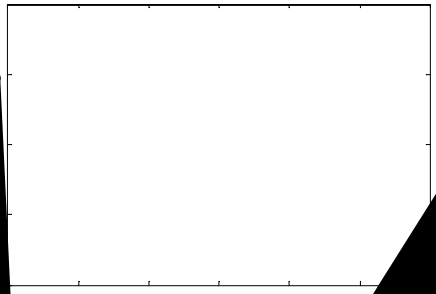

odelled velocity against me

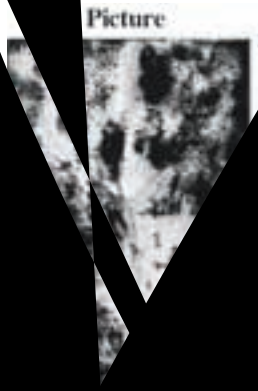

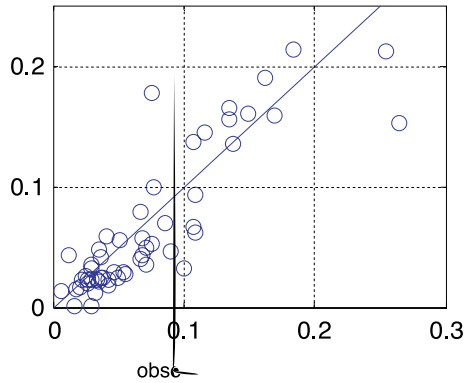

Figure 6. PSEM_2D modelled velocity with *ff* calculated from Eq. 12

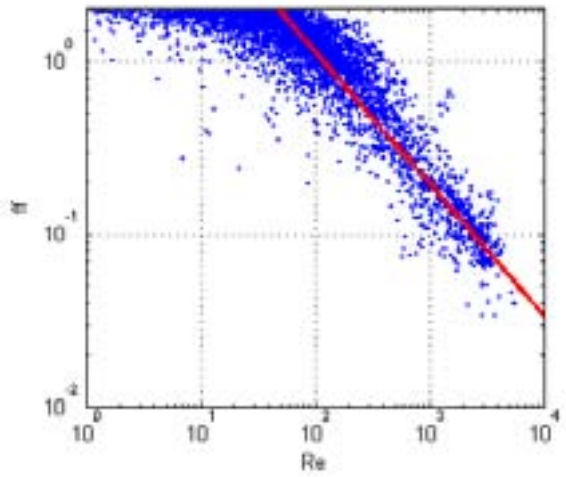

Figure 7. Relationship between Friction factor *ff* and Reynolds number *Re* simulated by PSEM_2D with friction factor calculated from Eq. 12

Figure 8. Relationship between Friction factor *ff* and Reynolds number *Re*: comparison with results from Nearing et al. (1997)

Discussion and Conclusion

The SVG technology has allowed flow-velocity measurement in a wide range of flow speeds (from 0·006m ·s^{-1} to 0·27·s^{-1} in this experiment). The use of salty brine as a tracer makes SVG suitable for measuring very shallow flows. The only limitation was the probe size, which was 1-cm wide and 10-cm long. Thanks to this technology, we were able to measure velocity in a wide variety of flow conditions, from unconcentrated to concentrated in a small rill, from laminar to turbulent, and from subcritical to supercritical. The data obtained have been used to test three hydrological models (PSEM_2D, NCF, and RillGrow2) which were very different to each other, having only in common the use of a Manning/Darcy-Weisbach-type hydraulic equation with a constant, homogeneous friction factor. The main results were the followings:

- PSEM_2D, NCF and RillGrow2 to a lesser extent, simulated satisfactorily the patterns of flow velocity and Reynolds number *Re*. However, both patterns and values of the Froude number *Fr* were incorrectly predicted by the three models.
- Low velocities were overestimated (PSEM_2D NCF). High velocities were largely under-estimated (all models).
- *Re* values estimated by the models are realistic. However, the classical threshold of *Re* = 2,000 for the transition between laminar to turbulent flow, would predict laminar flow everywhere on the plot but in the central channel, while field observation described turbulence even in the tributaries of the main channel.
- A heterogeneous friction factor *ff* was calculated to fit the modelled velocity with the whole range of observed values. Running PSEM_2D with the new *ff* led to an improvement of *Re* and *Fr* patterns. Moreover, *ff* appeared to be related to *Re* via a power law similar to the one observed by Nearing *et al.* (1997) on sandy bare soil (albeit the range of *ff* and *Re* differed in the two studies).

These results lead to the following conclusions:

- The hydrograph alone is an insufficient source of information to calibrate *ff*. Other source of data such as the measured velocity field is therefore highly desirable to calibrate any hydrological model dedicated to be coupled to an erosion model.
- *ff* decreases with increasing *Re*, which we interpreted by the fact that the flow becomes less sensitive to the grain roughness when its

turbulence increases. This result confirms the conclusion of Nearing *et al.* (1997) for sandy bare soils and extends them to lower values of *Re* than in their study.

- The usual procedure in soil-erosion models is the calibration, from the hydrograph, of a single value of *ff* for the whole plot. Our results show that this procedure will correctly calibrate the friction factor for the cells at low to moderate velocity, which dominate the hydrological response of the plot. Contrarily, the hydrograph will not be significantly affected by an even dramatic underestimation of the highest velocity because these maxima occur on short distances, so that the corresponding error in terms of travel time will be small.
- Uniform *ff* leads to erroneous *Fr*. However, when measured velocities are used to recalculate *ff, Fr* patterns and values are satisfying. Gimenez *et al.* (2004) have demonstrated the importance of *Fr* in the initiation and the development of rills. Any future model aimed at simulating rill initiation on the basis of these findings will first have to account for the *ff-Re* relationship in order to have realistic simulations of *Fr* for using at predicting rill initiation.

Acknowledgements

This work was granted by the RIDES project, an ECCO research program. The new miniaturized version of SVG has been developed in a collaborative project between The Institut de Recherche pour le Développement (IRD) and the USDA-ARS National Soil Erosion Laboratory (NSERL). The authors want to thank Dr. Chi Hua Huang, from NSERL, for his support and helpful advices in the development of SVG. The rainfall simulations have been conducted by Kokou Abotsi, from IRD Dakar, Senegal.

References

Abrahams, A.D., Anthony, J.P. and Wainwright, J., 1995. Effects of vegetation change on interrill runoff and erosion, Walnut-Gulch, Southern Arizona. *Geomorphology*, **13**, 37-48.

Desmet, P.J.J. and Govers, G., 1997. Two-dimensional modelling of the within-field variation in rill and gully geometry and location related to topography. *Catena*, **29**, 283-306.

Esteves, M., Planchon, O., Lapetite, J.M., Silvera, N. and Cadet, P., 2000a. The 'EMIRE' large rainfall simulator: Design and field testing. *Earth Surface Processes and Landforms*, **25**, 681-690.

Esteves, M., Faucher, X., Galle, S., Vauclin, M., 2000b. Overland flow and infiltration modelling for small plots during unsteady rain: numerical results versus observed values. *Journal of Hydrology* **228**, 265-282.

Favis-Mortlock, D., 1998. A self-organizing dynamic systems approach to the simulation of rill initiation and development on hillslopes. Computers & Geosciences, **24**(4), 353-372.

Favis-Mortlock, D.T., Boardman, J., Parsons, A.J. and Lascelles, B., 2000. Emergence and erosion: a model for rill initiation and development. Hydrological Processes, **14**, 2173-2205.

Gilley, J.E., L.J. Lane, J.M. Laflen, H.D. Nicks and W.J. Rawls. 1988. USDA-water erosion prediction project: New generation erosion prediction technology. In: Modeling, Agricultural, Forest, and Rangeland Hydrology. Symposium Proceedings. Pub. 07-88:260-263. Available from Am. Soc. Agric. Eng., St. Joseph, MI.

Gilley, J.E., Kottwitz, E.R., Simanton, J.R., 1990. Hydraulic characteristics of rills. *Trans. Am. Soc. Agric. Eng.* **33**, 1900-1906.

Gimenez, R. and Govers, G., 2001. Interaction between bed roughness and flow hydraulics in eroding rills. *Water Resources Research*, **37**, 791-799.

Gimenez R., Planchon O., Silvera N., Govers G. 2004. Longitudinal velocity patterns and bed morphology interaction in a rill. *Earth Surface Proccesses and Landforms* **29**, 105-114.

Govers, G., 1992. Relationship between discharge, velocity and flow area for rills eroding loose, nonlayered materials. *Earth Surface Processes and Landforms*, **17**, 515-528.

Grant, G.E., 1997. Critical flow constrains flow hydraulics in mobile-bed streams: A new hypothesis. *Water Resources Research*, **33**, 349-358.

Green, W.H. and Ampt, G.A. 1911. Studies on soil physics: 1, flow of air and water through soils. *Journal Agric. Sciences* **4**, 1-24.

Hayami S. 1951. On the Propagation of Flood Waves. Disaster Prevention Research Institute, Kyoto University, Japan, Bulletin no. 1.

Henderson, F.M. 1966. Open Channel Flow. New York: Macmillan Company.

MacCormack, R.W. 1969. The effect of viscosity in hypervelocity impact cratering. New-York, American Institute of Aeronautics and Astronautics.

Nearing, M.A., Norton, L.D., Bulgakov, D.A., Larionov, G.A., West, L.T. and Dontsova, K.M., 1997. Hydraulics and erosion in eroding rills. *Water Resources Research*, **33**, 865-876.

Nord, G. and M. Esteves. in press. PSEM_2D: a physically-based model of erosion processes at the plot scale. *Water Resources Research*.

Parsons, A.J., Wainwright, J., Abrahams, A.D. and Simanton, J.R., 1997. Distributed dynamic modelling of interrill overland flow. Hydrological Processes, **11**(14), 1833-1859.

Parsons, A.J., Wainwright, J., Powell, D.M., Kaduk, J. and Brazier, R.E. 2004. A conceptual model for understanding and predicting erosion by water, *Earth Surface Processes and Landforms* **29**, 1293-1302.

Pilotti, M. and Menduni, G. 1997. Application of lattice gas techniques to the study of sediment erosion and transport caused by laminar sheetflow. *Earth Surface Processes and Landforms*, **22**, 885-893.

Planchon O., Silvera N., Gimenez R., Favis-Mortlock D., Wainwright J., Lebissonnais Y., Govers G. 2005. Estimation of flow velocity in a rill using an automated salt-tracing gauge. *Earth Surface Proccesses and Landforms*. **30**, 833-844.

Planchon, O. and Darboux, F., 2001. A fast, simple and versatile algorithm to fill the depressions of digital elevation models. Catena, **46**(2-3), 159-176.

Planchon, O., Esteves, M., Silvera, N. and Lapetite, J.M., 2001. Microrelief induced by tillage: measurement and modelling of Surface Storage Capacity. Catena, **46**(2-3), 141-157.

Savat, J., 1980. Resistance to flow in rough supercritical sheet flow. *Earth Surface Processes*, 103-122.

Scoging, H. 1992. Modelling overland-flow hydrology for dynamic hydraulics. Overland Flow Hydraulics and Erosion Mechanics. A.J. Parsons and A.D. Abrahams. London, UCL Press, 89-103.

Siepel, A.C., Steenhuis, T.S., Rose, C.W., Parlange, J.Y. and McIsaac, G.F., 2002. A simplified hillslope erosion model with vegetation elements for practical applications. *Journal of Hydrology*, **258**, 111-121.

Wainwright, J., Parsons, A.J. and Abrahams, A.D., 1999. Field and computer simulation experiments on the formation of desert pavement. *Earth Surface Proccesses and Landforms*. **24**: 1025-1037.

Zhang, W. and T.W. Cundy. 1989. Modelling of two dimensional overland flow. *Water Resources Research* **25**, 2019-2035.

Management of Tropical Sandy Soils for Sustainable Agriculture

A holistic approach for sustainable development of problem soils in the tropics

27th November - 2nd December 2005
Khon Kaen, Thailand

Proceedings

Organizing Committee:

Christian Hartmann (IRD/LDD)	Chairman
Narong Chinabut (LDD)	co-Chairman
Andrew Noble (IWMI)	Secretary
Yuji Niino (FAO)	Treasurer
Taweesak Vearasilp (LDD)	co-Secretary
Anan Polthanee (KKU)	co-Secretary
Roland Poss (IRD)	co-Secretary

Scientific committee:

AndrŽBationo	(CIAT, Kenya)
Richard Bell	(Murdoch University, Australia)
Sue Berthelsen	(CSIRO, Australia)
Eric Blanchart	(IRD, France)
Ary Bruand	(ISTRO, France)
John Caldwell	(JIRCAS, Thailand)
Suraphol Chandrapatya	(IWMI, Thailand)
Hari Eswaran	(USDA, USA)
Martin Fey	(Stellenbosh University, South Africa)
Alfred Hartemink	(ISRIC, The Netherlands)
Christian Hartmann	(IRD, Thailand)
Irb Kheoruenromne	(Kasetsart University, Thailand)
Phil Moody	(Dep. Natural Resources and Mines, Australia)
Paul Nelson	(James Cook University, Australia)
Andrew Noble	(IWMI, Thailand)
William Payne	(Texas A&M University, USA)
Roland Poss	(IRD, France)
Robert Simmons	(IWMI, India)
Christian Valentin	(IRD, Laos)
Bernard Vanlauwe	(CIAT-TSBF, Kenya)
Hidenori Wada	(Japan)
Toshiyuki Wakatuki	(Kinki University, Japan)
Wanpen Wiriyakitnateekul	(LDD, Thailand)

Cover Design by: Prayud Chmapalin

ISBN 978-974-7946-96-3

For copies write to: Yuji Niino
Land Management Officer
FAO Regional Office for Asia and the Pacific
Maliwan Mansion, 39 Phra Atit Road
Bangkok 10200
THAILAND
Tel: (+66) 2 697 4000
Fax: (+66) 2 697 4445
E-mail: Yuji.Niino@fao.org

Under the auspices of:
International Union of Soil Science (IUSS)

organized by:
L'Institut de Recherche pour le Développement (IRD, France)
Land Development Department (LDD, Thailand)

co-organized by:
International Water Management Institute (IWMI)
Food and Agriculture Organization of the United Nations (FAO)
University of Khon Kaen, Faculty of Agriculture (KKU)

supported by:
CSIRO Land and Water, Australia
UNCCD
ISRIC